Bulletin of the Seismological Society of America, Vol. 86, No. 4, pp. 1061–1076, August 1996

An Analysis of Simulated and Observed Blast Records in the Salt Lake Basin

by Kim B. Olsen,* James C. Pechmann, and Gerard T. Schuster

Abstract We have simulated 0.2 to 1.2-Hz 3D elastic wave propagation in the Salt Lake Basin from a blast at a nearby open-pit mine. A fourth-order staggered-grid finite-difference method was used to simulate the blast in a two-layer basin model (58 × 43 × 9 km) consisting of semiconsolidated sediments up to 1.3-km thick surrounded by bedrock.

Data from four blasts in the mine pit, recorded by a network of 10 digital three-component instruments, were compared to the results of the simulation. The simulation reproduces the overall pattern of ground-motion amplification at basin sites relative to a rock site, as measured by ratios of peak particle velocities, cumulative kinetic energies, and spectral magnitudes. Considering the simple two-layer basin model used in the 3D simulation, this finding suggests that the deep 3D basin structure significantly contributes to low-frequency ground-motion amplification in the Salt Lake Basin.

Order-of-magnitude discrepancies exist between some of the observed and predicted ground-motion parameters, and the simulations underpredict the signal durations at most stations. We use 2D simulations along a profile through the southern part of the basin model to investigate the causes of these discrepancies. These causes may be summarized, in order of their importance along this profile, as follows:

1. Effects of a near-surface layer of low-velocity unconsolidated sediments (*P*- and *S*-wave velocities of 1.65 and 0.41 km/sec, respectively) that at soil sites along the profile increase the peak particle velocities by up to a factor of 3 and significantly increase the ground-motion durations.
2. Attenuation in the sediments, which greatly diminishes the ground-motion durations on the synthetic seismograms when parameterized by realistic values of the quality factor, Q (20 for soil sites and 35 for bedrock sites).
3. 2D topographic scattering, which increases the peak particle velocities by up to a factor of 2 and increases the signal durations for sites along the profile.

Compared to the records from the simple two-layer 3D simulation, the records from a 2D *P/SV*-wave simulation that includes processes (1) through (3) provide a better match to the blast data—especially the observed durations of shaking. At five of the six stations along the profile, the 2D simulation reproduces the normalized radial and vertical peak particle velocities to within a factor of 2 and the normalized cumulative kinetic energies and spectral amplitudes on these components to within generally a factor of 3.

Our results suggest that deep-basin resonance, reverberations in the near-surface low-velocity layer, attenuation, and topographic scattering significantly influence site amplification in the Salt Lake Basin. Future studies of site amplification in the Salt Lake Basin should include the effects of all of these mechanisms.

*Present address: Institute for Crustal Studies, University of California at Santa Barbara, Santa Barbara, California 93106-1100.

Introduction

A series of 2D modeling studies (Benz and Smith, 1988; Murphy, 1989; Hill *et al.,* 1990) have been carried out to investigate the causes of low-frequency seismic wave amplification in the Salt Lake Valley, Utah. These studies used a variety of seismic sources, including vertically incident plane *P* and *SH* waves and explosion and double-couple line sources buried beneath the valley. In these 2D simulations, the ground-motion amplification was the largest above the deepest parts of the basin and was due in part to large-amplitude surface waves generated by body waves striking the edges of the basin. Soil/rock spectral ratios calculated from the 2D synthetics generally underpredicted spectral ratios calculated from nuclear blasts recorded at distances of 500 to 600 km by stations in the Salt Lake Valley (King *et al.,* 1983, 1987), in some cases by more than a factor of 2. However, the source locations used in the 2D simulations were quite different from the locations of the nuclear blasts. These earlier studies did not take into account the effects of *S*-wave velocities as low as 0.27 km/sec in the unconsolidated sediments of the Salt Lake Basin (see Williams *et al.,* 1993), attenuation, or 3D scattering, but they did demonstrate the important effects of the deep basin structure (down to 1.5 km in depth) on seismic wave amplification in the Salt Lake Valley.

A new generation of faster computers allows us to now include additional features in the modeling of wave propagation in the Salt Lake Basin. Specifically, the 3D low-frequency seismic response of the Salt Lake Basin model can now be computed, as has been done for models of several sedimentary basins in California (Frankel and Vidale, 1992; Frankel, 1993: Graves, 1993; Yomogida and Etgen, 1993; Olsen *et al.,* 1995b; Olsen and Archuleta, 1996). Olsen *et al.* (1995a) have computed the seismic response of a 3D Salt Lake Basin model to vertically and horizontally incident plane *P* waves, and Olsen and Schuster (1995) have analyzed the salient causes of strong ground motion amplification for the case of the vertically incident *P*-wave source. Olsen and Schuster (1995) found that 2D and especially 1D synthetics generally underestimate the ground-motion parameters predicted by 3D modeling. However, Olsen *et al.* (1995a) showed that simulations in complex 2D models can provide more accurate predictions of seismic wave amplification in the Salt Lake Basin than simulations with a simple two-layer 3D basin model. Their complex 2D models included topography, the near-surface low-velocity unconsolidated sediments, and attenuation.

How close to reality is our current 3D modeling of seismic wave propagation in the Salt Lake Basin, and therefore, how close are we to accurately predicting low-frequency ground motions in the Salt Lake Valley? To answer this question, this article compares the results of a 3D elastic simulation of a Bingham Mine blast to observed blast recordings. Velocity seismograms and ground-motion parameter ratios for the simulated records are compared to seismic data from four blasts recorded at 10 stations within the Salt Lake Valley. We also use 2D simulations to examine whether the discrepancies between the simulated and observed records can be explained by known model deficiencies, such as the omission of topography, the near-surface low-velocity layer, and attenuation. Our objective in this article is to assess the accuracy of purely deterministic ground-motion predictions done using presently available information on the subsurface velocity and density structure.

This article is divided into five sections. The first section describes the 3D Salt Lake Basin model, the finite-difference scheme, and the numerical representation of the blast. The second section analyzes snapshots of simulated wave propagation in the Salt Lake Basin model. The collection and processing of blast data from the Bingham Mine are described in the third section. In the fourth section, we compare synthetic seismograms and ground-motion parameter ratios for the simulation of a Bingham Mine blast to corresponding data from blasts recorded in the Salt Lake Valley. Finally, we examine how site amplification is affected by topography, a near-surface low-velocity layer, and attenuation.

Simulation of Mine Blast

Salt Lake Basin Model

The 3D model of the Salt Lake Basin used in this study (Fig. 1) consists of sediments surrounded by bedrock; the boundary between sediments and bedrock was estimated by 3D inversion of gravity data, constrained by three seismic reflection lines and 40 water well logs (Radkins, 1990). The northern part of the basin model is the best constrained, because all three seismic reflection lines are located in the northern part of the valley. The model is less reliable in the southwestern part of the basin, where recent seismic refraction studies suggest that the thickness of the sediments is underestimated by up to 0.4 km in some places (C. Zhou, personal comm., 1993).

Hill *et al.* (1990) and Murphy (1989) included three layer boundaries in their 2D Salt Lake Basin models: R1, separating unconsolidated and semi-consolidated sediments; R2, separating semi-consolidated and consolidated sediments; and R3, separating consolidated sediments and bedrock. Their 2D simulations indicated that low-frequency amplification in the Salt Lake Valley is controlled primarily by the R1 and R2 boundaries. Since the R2 boundary is associated with the largest velocity and density contrasts and is the interface modeled by Radkins (1990) using gravity data, we choose to use this interface to separate sediments and bedrock in our model. The low-velocity unconsolidated sediments are omitted in our 3D model because of the large amounts of CPU time and memory needed to include them.

The density and *P*-wave velocity values of the bedrock are taken from Hill *et al.* (1990), who obtained them from well logs. The *P*-wave velocity of the sediments was taken to be 2.2 km/sec, 10% lower than that given by Hill *et al.*

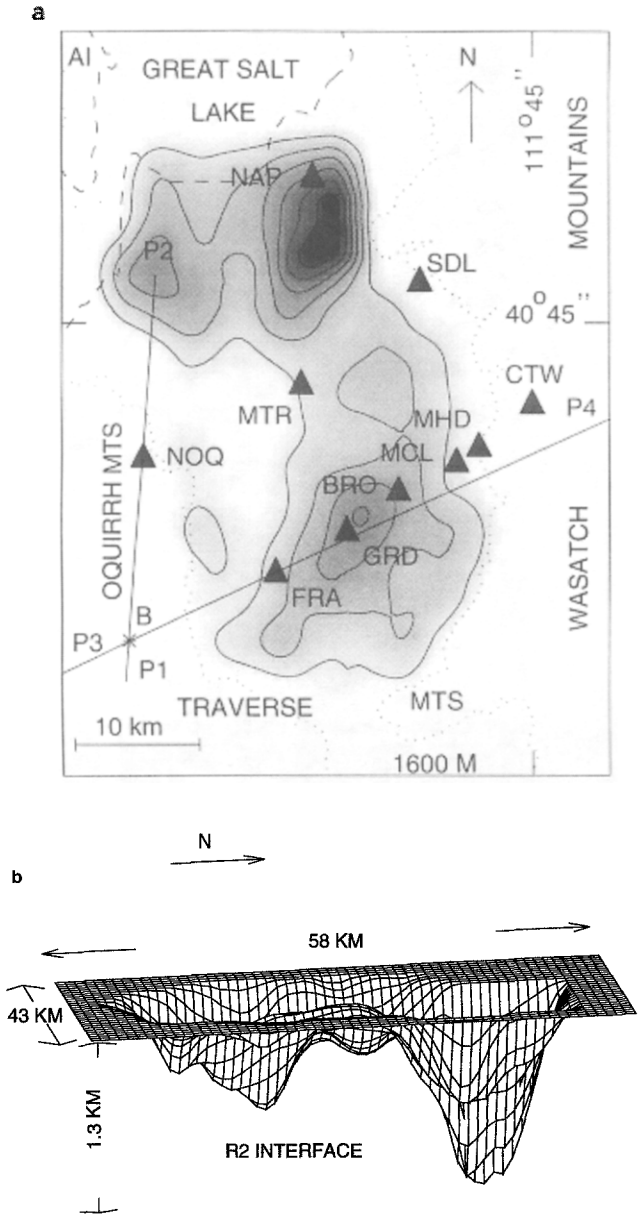

Figure 1. Salt Lake Basin model. (a) Map of the Salt Lake Basin. The contours (200-m interval, shallowest contour at a depth of 150 m below the valley floor) and the shading depict the depth of the R2 interface (the sediment-bedrock boundary) below the valley floor; darker shading indicates greater depth to R2. The dotted and dashed lines depict an elevation of 1600 m above sea level and the shoreline of the Great Salt Lake, respectively. AI is Antelope Island, and B is the Bingham Canyon Copper Mine. The triangles labeled with three-letter codes denote the locations of recording sites. The lines P1-P2 and P3-P4 depict the locations of the cross sections used for the 2D modeling. (b) Three-dimensional perspective of the R2 interface. Table 1 lists the 3D modeling parameters.

(1990) for the semi-consolidated sediments. The lower velocity for the semi-consolidated sediments was a compromise between excluding the unconsolidated sediments and keeping the sediment velocity within limitations dictated by the computational power available to us.

S-wave velocities are approximated by dividing the *P*-wave velocities by $\sqrt{3}$. Nicholson and Simpson (1985) found this approximation to be reasonable for bedrock deeper than $\approx$2 to 3 km by analyzing *P* and *S* arrival times from microearthquakes; however, they also found that V_p/V_s ratios in rock typically increase to values of around 2.0 at shallower depths.

Finite-Difference Scheme

We use a staggered-grid finite-difference scheme to solve the 3D elastic equations of motion (Levander, 1988) to a level of accuracy that is fourth order in space and second order in time. The numerical implementation of the 3D scheme is described in Olsen (1994, Appendix A of Chapter 1). The simulation was carried out on an IBM 3090 supercomputer using approximately 320 Mbytes of physical memory.

The basin model is discretized with a grid point spacing of 0.15 km. This spacing corresponds to approximately seven grid points per minimum shear wavelength of 1.1 km, which limits the numerical dispersion error to less than 12% (see Olsen, 1994, Appendix B of Chapter 1). The Salt Lake Basin model (approximately 58 × 43 × 9 km) is discretized into 384 × 288 × 60 (=6.6 million) grid points. The sides of the computational model are padded with homogeneous regions of attenuative material that limit reflections from the boundaries of the grid (Cerjan *et al.*, 1985). The 3D modeling parameters are listed in Table 1.

Table 1
3D Modeling Parameters

Spatial discretization (km)	0.15
Temporal discretization (sec)	0.013
P-wave velocity of sediments (km/sec)	2.20
S-wave velocity of sediments (km/sec)	1.27
Density of sediments (g/cm^3)	2.2
P-wave velocity of bedrock (km/sec)	5.00
S-wave velocity of bedrock (km/sec)	2.89
Density of bedrock (g/cm^3)	2.6
Number of E–W grid points	288
Number of N–S grid points	384
Number of vertical grid points	60
E–W extent of model (km)	43
N–S extent of model (km)	58
Vertical extent of model (km)	9
Minimum source frequency (Hz)	0.2
Maximum source frequency (Hz)	1.2
Peak source frequency (Hz)	0.6
Number of time steps	4616
Simulation time (sec)	60

Source Function

The typical blast configuration at the Bingham Mine pit consists of five rows of holes loaded with dynamite to a maximum depth of 58 ft. The surface area covered by a blast is approximately 135 × 30 m. The charges in a single row are exploded simultaneously, and the time delay between explosions in adjacent rows is 35 msec. Since the Salt Lake Basin is discretized with a grid spacing of 150 m, the Bingham Mine blast can be approximated as a point source. The point source was implemented by adding the Ricker wavelet pressure-time history shown in Figure 2 to the normal stresses of a free-surface grid point. The source spectrum has a peak frequency of 0.6 Hz and a bandwidth of approximately 0.2 to 1.2 Hz (Fig. 2).

Analysis of Simulated Wave Propagation

In this section, we use snapshots of particle velocities to analyze approximately 30 sec of low-frequency wave propagation in our Salt Lake Basin model for a simulated blast at the Bingham Mine (Fig. 3). The radial- and vertical-component snapshots at 5.2 sec show the relatively weak *P* wave and much stronger Rayleigh wave generated at the source. The small amount of energy on the transverse-component snapshot is an artifact caused by source discretization. At 10.4 sec, the waves that have entered the basin and propagated in the sediments lag slightly behind those in the surrounding faster bedrock. The Rayleigh wave is followed by a wake of scattered waves in the basin sediments that becomes much more pronounced in the later snapshots. Note the increased amount of energy appearing in the snapshots of the transverse component after 15.6 sec. This energy is generated by reflections and mode conversion at the sediment-bedrock interface and/or the free surface. The weak

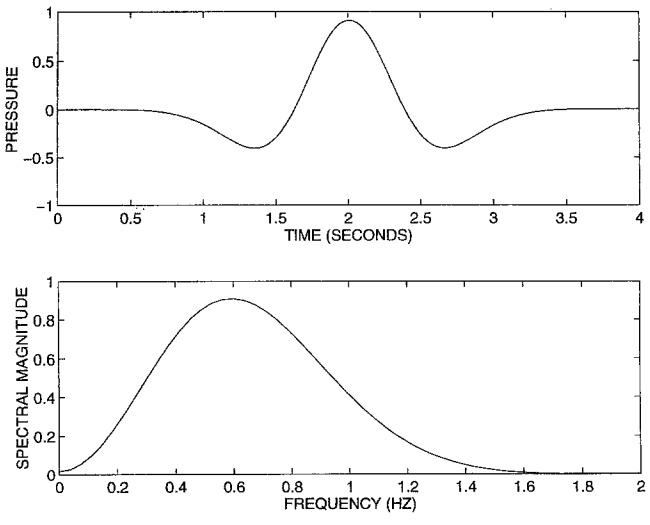

Figure 2. Pressure-time function (top) and amplitude spectrum (bottom) of the Ricker wavelet source function used in the 3D simulations.

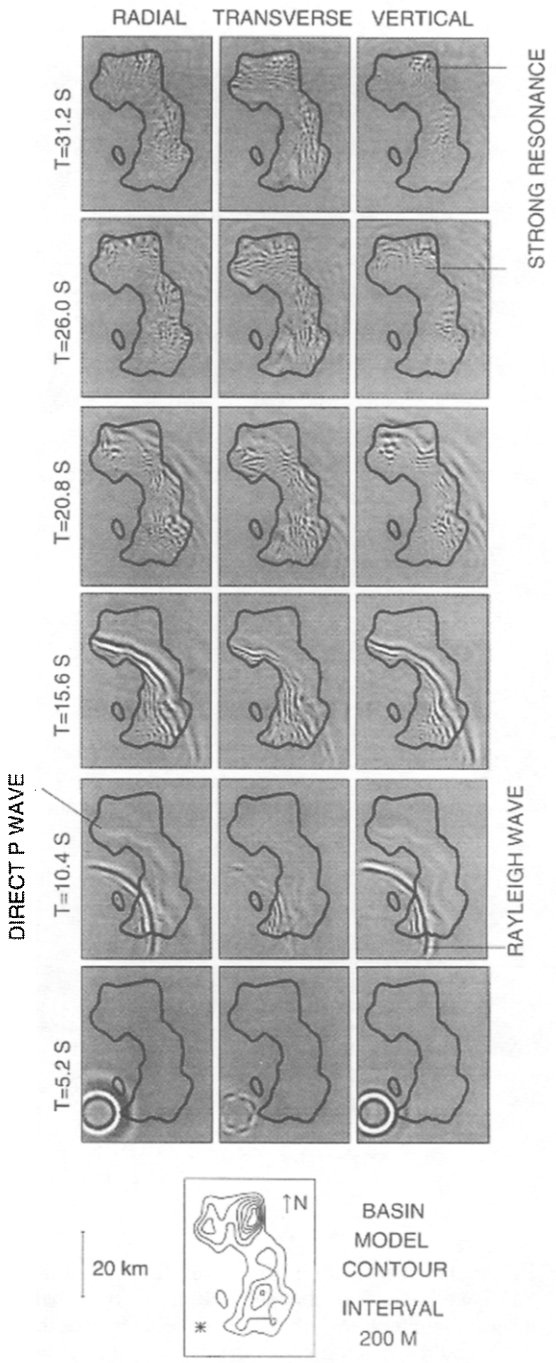

Figure 3. Snapshots of simulated wave propagation in the Salt Lake Basin for a Bingham Mine blast; the snapshots depict radial-, transverse-, and vertical-component velocities at 5.2-sec intervals for approximately 30 sec of wave propagation after the origin time of the blast. Light (dark) shading depicts negative (positive) velocity. The thick line shown on the snapshots depicts the outline of the basin model. The contour map at the bottom shows the depth to the R2 interface at a contour interval of 200 m, with the shallowest contour at a depth of 150 m below the valley floor; the star depicts the location of the blast. The particle motion is scaled by the same constant for all snapshots.

direct *P* wave has left the basin by 15.6 sec. At 20.8 sec, the strongest ground motion in the basin is no longer associated with the direct Rayleigh wave, which is about to leave the basin through its northern and eastern boundaries; hereafter, the strongest shaking takes place in the deeper parts of the basin. At 26.0 and 31.2 sec, the energy resonates strongly in the deeper parts of the basin, especially on the vertical component.

Recording and Processing of Blast Data

We compare our synthetic seismograms to records of four Bingham Mine blasts that were recorded during March and April of 1992 (Table 2). The blast records are from 10 temporary three-component stations, of which six are located on unconsolidated sediments in the Salt Lake Valley and four are located on bedrock outcrops in the surrounding mountains (Fig. 1 and Table 3).

The equipment at each station consisted of a REF-TEK digital recorder and three Geotech S-13 velocity transducers. The frequency response of the recorders is flat and phaseless up to 10 Hz when they are operated at a sampling rate of 25 Hz, the rate used for the blast recordings. The free periods of the seismometers were all set to 1.0 sec, and weight-lift tests showed that all of them had gains and damping factors within 5% and 10%, respectively, of their average values. To allow for comparison with the synthetic seismograms, we deconvolved the nominal seismometer response from all of the data traces to obtain velocity seismograms over the frequency range 0.1 to 10 Hz and then convolved the traces with the Ricker wavelet source-time function used to generate the synthetics. The rationale for this procedure is that the source duration times of the actual Bingham Mine blasts are much shorter than the shortest period used in the 3D simulations (0.8 sec), so that the source-time functions of these blasts can be approximated by delta functions.

Table 2
Origin Times and Locations of the Bingham Mine Blasts*

Code	Date (m/d/y)	Origin Time (UTC)	Lat (N) (Deg Min)	Long (W) (Deg Min)
B0328	3/28/92	2220 15.00	40 31.04	112 09.98
B0331	3/31/92	1751 08.28	40 31.82	112 09.82
B0405	4/05/92	1957 31.06	40 31.24	112 09.96
B0411	4/11/92	1910 07.57	40 30.95	112 10.27

*Determined from *P*-wave arrival times recorded at bedrock sites around the Salt Lake Valley.

Table 3
Stations Used to Record Seismic Waves from the Bingham Mine Blasts

Code	Lat (N)	Long (W)	Elev (m)	Surface Material*
BRO	40 37.67	111 52.72	1337	Stream alluvium
CTW	40 41.55	111 45.02	1731	Quartzite bedrock
FRA	40 34.08	111 59.62	1441	Lacustrine clay and silt
GRD	40 35.90	111 55.55	1323	Lacustrine clay and silt
MCL	40 38.94	111 49.32	1356	Stream alluvium
MHD	40 39.64	111 48.05	1597	Quartzite bedrock
MTR	40 42.41	111 58.18	1292	Lacustrine, marsh, and alluvium deposits
NAP	40 51.44	111 57.52	1283	Marsh and lacustrine deposits
NOQ	40 39.15	112 07.22	1622	Limestone bedrock
SDL	40 46.94	111 51.38	1567	Conglomerate bedrock

*Geological information for bedrock sites is from field observations; information for alluvium sites is from Personius and Scott (1992). All instruments were installed on a concrete pad inside an 45-cm deep, 75-cm diameter galvanized steel barrel.

Comparison of Simulated and Observed Blast Records

This section examines the successes and failures of using a 3D simulation to predict amplification of ground motions in the Salt Lake Basin from Bingham Mine blasts. We compare the 3D simulations to seismic data from four different blasts recorded at 10 sites in and near the Salt Lake Valley.

Velocity Seismograms

Figure 4 compares simulated (3D) and observed (O1 through O4) velocity seismograms for Bingham Mine blasts. The observed traces were aligned with the simulated ones on this figure using the strong arrival at 8 sec on the radial component at FRA. The amplitude scale is the same for all of the simulated traces, except as indicated on the figure. The observed traces are scaled separately for each blast to make the peak particle velocity of the observed radial seismogram at the nearest rock site, NOQ, match that of the corresponding 3D synthetic.

The observed seismograms at any one site show a rough agreement in the maximum amplitudes and signal durations of significant wave trains. This observation suggests that the 0.2 to 1.2-Hz ground motion is not very sensitive to the blast location within the Bingham Mine pit—as expected, because the dominant wavelength of the slowest phase (the Rayleigh wave) propagating in the bedrock is approximately 4.5 km, which is larger than the diameter of the open-pit mine ($\approx$3 km).

We note that the agreement between the simulated and observed waveforms is not particularly good at most stations. The best match in wave shape is for the direct waves on the radial and vertical components at FRA. The signal durations of the simulated seismograms generally underpredict those of the observed seismograms, especially at the alluvium sites in the southern and central parts of the basin (FRA, GRD, BRO, MCL, and MTR). Possible reasons for these discrepancies include the omission from the basin model of topography, near-surface low-velocity sediments, and bedrock heterogeneities (lateral variations of density and/or velocity). The consequences of neglecting the first two of these model features are analyzed in a later section.

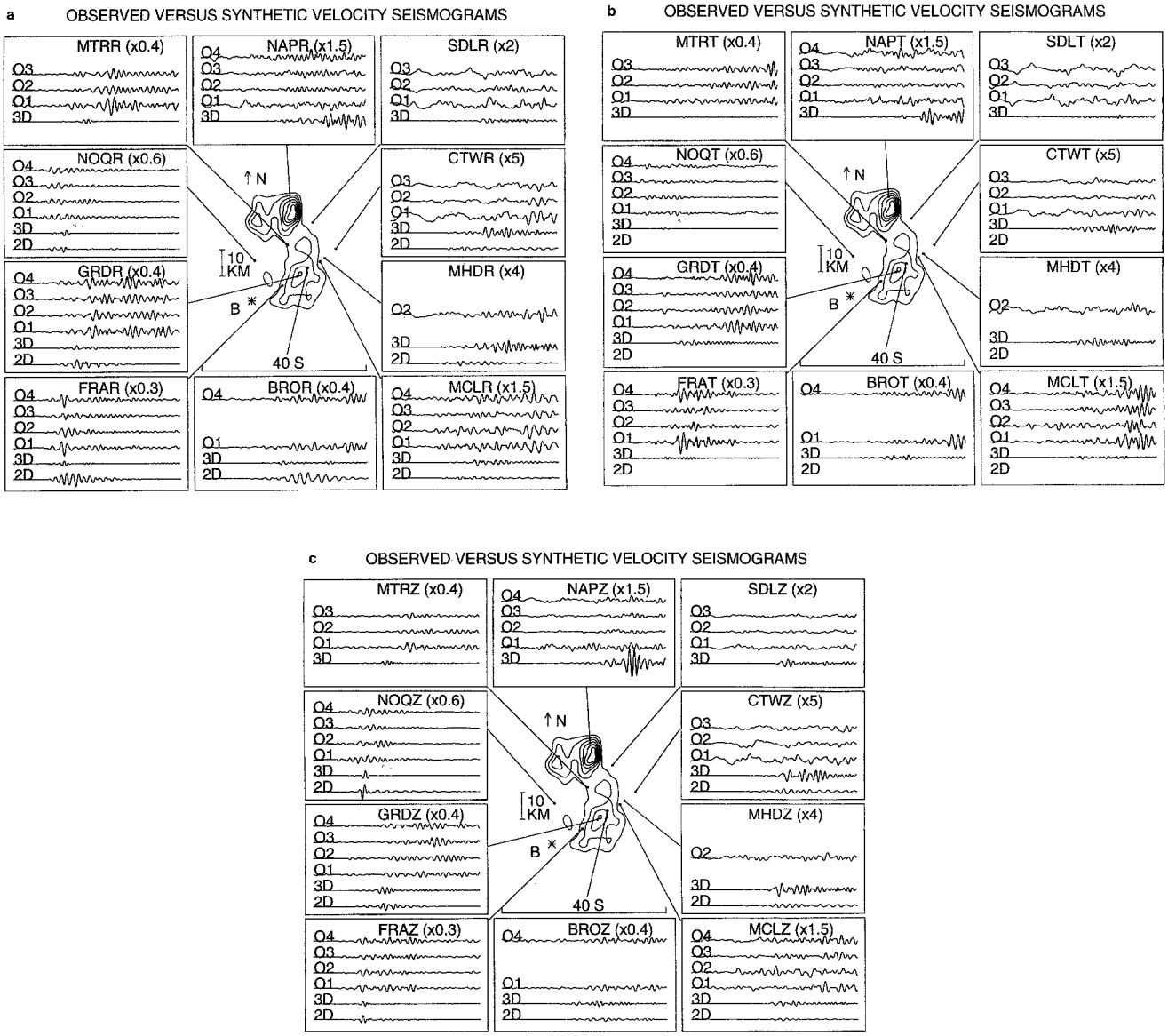

Figure 4. Comparison of simulated and observed velocity seismograms for Bingham Mine blasts at the 10 recording sites in the Salt Lake Valley: (a) radial components, (b) transverse components, and (c) vertical components. "3D" denotes synthetic traces simulated using the 3D Salt Lake Basin model. "2D" denotes synthetic traces simulated using 2D models. The 2D models are cross sections of the 3D model along profiles P1-P2 and P3-P4 (Fig. 1a) to which topography and a near-surface low-velocity layer in the sediments have been added. The 2D traces have been transformed into point source seismograms and corrected for attenuation (Q equal to 20 and 35 for soil and bedrock sites, respectively). O1 through O4 denote, respectively, observed blasts B0328, B0331, B0405, and B0411 (Table 2). The observed seismograms are convolved with the Ricker wavelet source function used in the numerical simulations. Amplitude scaling factors have been applied to each set of seismograms to make the peak radial velocities match at NOQ, the closest rock site to the blast. Additional scaling factors applied for plotting purposes only are indicated in parentheses. Missing traces are either excessively noisy data or else unavailable due to equipment malfunctions. B on the map denotes the location of the blast. The contours (200-m interval, shallowest contour at a depth of 150 m below the valley floor) depict the depth to the R2 interface.

Ground-Motion Parameters

We realize that exact prediction of waveforms from mine blasts recorded in the Salt Lake Valley is an unrealistic expectation, considering the simplicity of our model. A more realistic goal of the numerical simulations is to predict some of the key indicators of ground-motion amplification in the basin. In this section, we use the simulated records to compute the areal distribution of three measurements of amplification in the Salt Lake Basin—peak particle velocity, cumulative kinetic energy, and mean spectral magnitude between 0.2 and 1.2 Hz—relative to those at a rock site. These indicators, which will henceforth be referred to as ground-motion parameters, are then compared to those calculated from the data recorded in the valley.

The ground-motion parameters are defined as follows:

1. The peak particle velocity for the kth component measured at location (x, y) is defined as

$$P_k(x, y) = \text{MAX}(|\dot{u}_k(x, y, t)|), \tag{1}$$

where $\dot{u}_k(x, y, t)$ is the velocity-time history for the kth component, and MAX indicates the maximum value of $|\dot{u}_k(x, y, t)|$ for all time t.

2. The cumulative kinetic energy per unit volume of the kth-component trace is given as

$$E_k(x, y) = \frac{1}{2}\rho(x, y)\int \dot{u}_k^2(x, y, t)\, dt, \tag{2}$$

where $\rho(x, y)$ is the density and the limits of integration are over the time interval of the simulation. The density values given in Tables 1 and 4 were used to compute this quantity for both the data and the synthetics.

3. The spectral magnitude of the kth-component trace is defined as

$$S_k(x, y, \omega) = |\dot{U}_k(x, y, \omega)|, \tag{3}$$

where $\dot{U}_k(x, y, \omega)$ is the temporal Fourier transform of $\dot{u}_k(x, y, t)$. The last 5 sec of the seismic traces are tapered with a Hanning window prior to transformation into the frequency domain. The mean spectral magnitude is found by averaging the spectrum between 0.2 and 1.2 Hz.

The simulated parameters are normalized by dividing by the simulated radial-component parameters at NOQ, and the observed parameters are normalized by dividing by the observed radial-component parameters at NOQ for each blast.

Figure 5 depicts the normalized peak particle velocities, cumulative kinetic energies, and mean spectral magnitudes for the simulated Bingham Mine blast. The largest values of these ground-motion parameters are typically found near the source and above the deeper parts of the basin. Stronger ground shaking is expected over the deeper parts of the basin

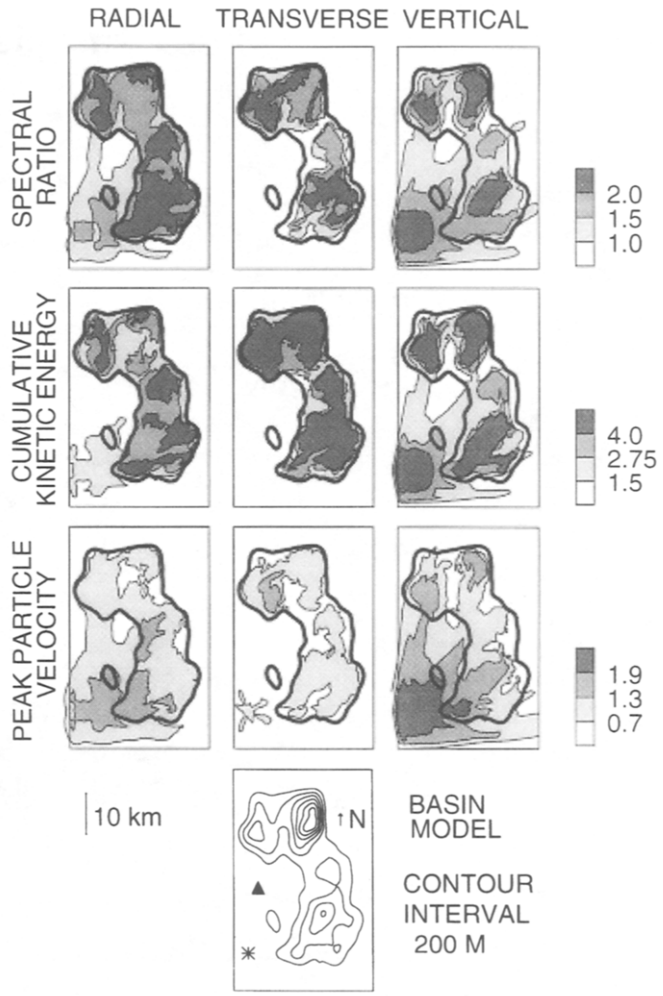

Figure 5. Ratios of peak particle velocities, cumulative kinetic energies, and mean spectral magnitudes in the Salt Lake Basin on the radial-, transverse- and vertical-component seismograms for a 3D simulation with a Bingham Mine blast. The values calculated for the radial component at NOQ are used as a reference. Closed contour lines with a perimeter length shorter than approximately 16 km are considered beyond the resolution of the model and have been discarded from the plots. The contour map at the bottom shows the depth to the R2 interface at a 200-m contour interval; the shallowest contour at a depth of 150 m (thick line) below the valley floor is superimposed on the ground-motion plots for reference. The locations of the blast and NOQ are depicted by a star and a triangle, respectively.

because the thicker sediments promote constructive interference of vertically propagating P and S waves in the source bandwidth of 0.2 to 1.2 Hz (see Olsen and Schuster, 1995).

Recall that the seismic waves radiated from our simulated blast produce motion primarily on the vertical and radial components. However, in some parts of the basin, values of the synthetic ground-motion parameters on the transverse component are larger than those on the radial and vertical components. This result is consistent with Figure 3, which

Peak Particle Velocity Ratios

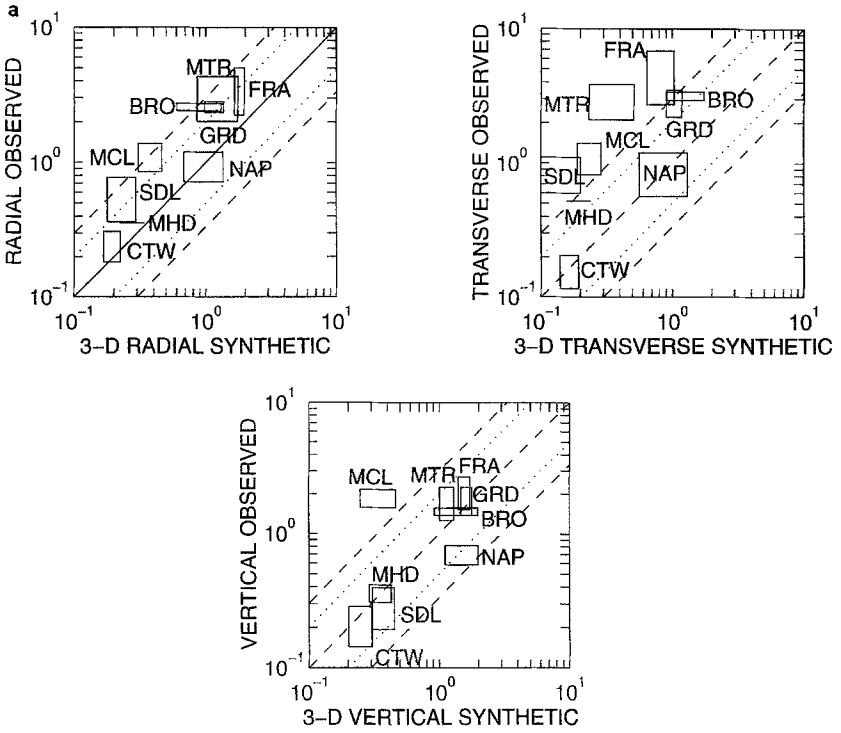

Cumulative Kinetic Energy Ratios

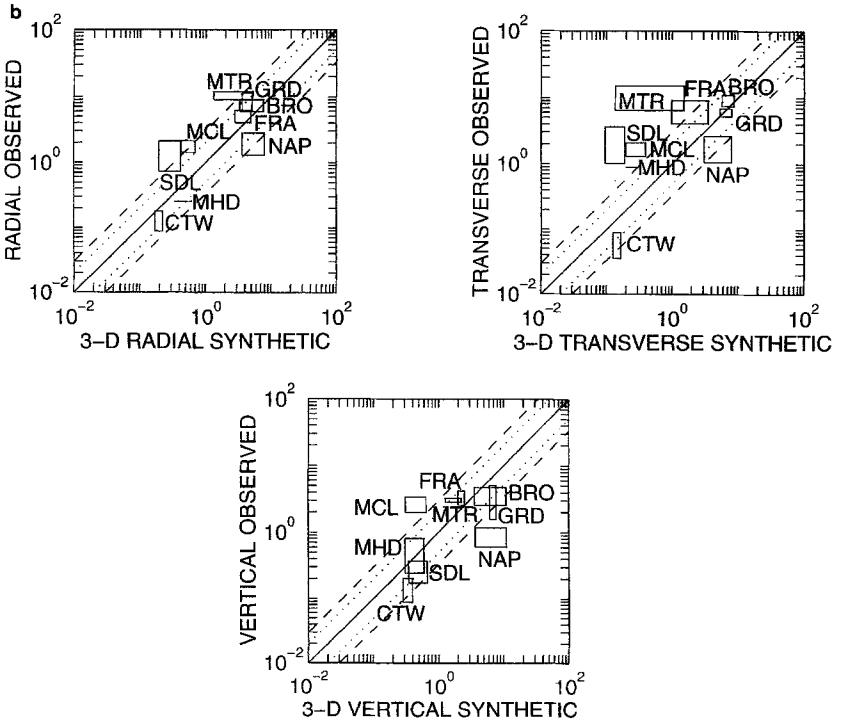

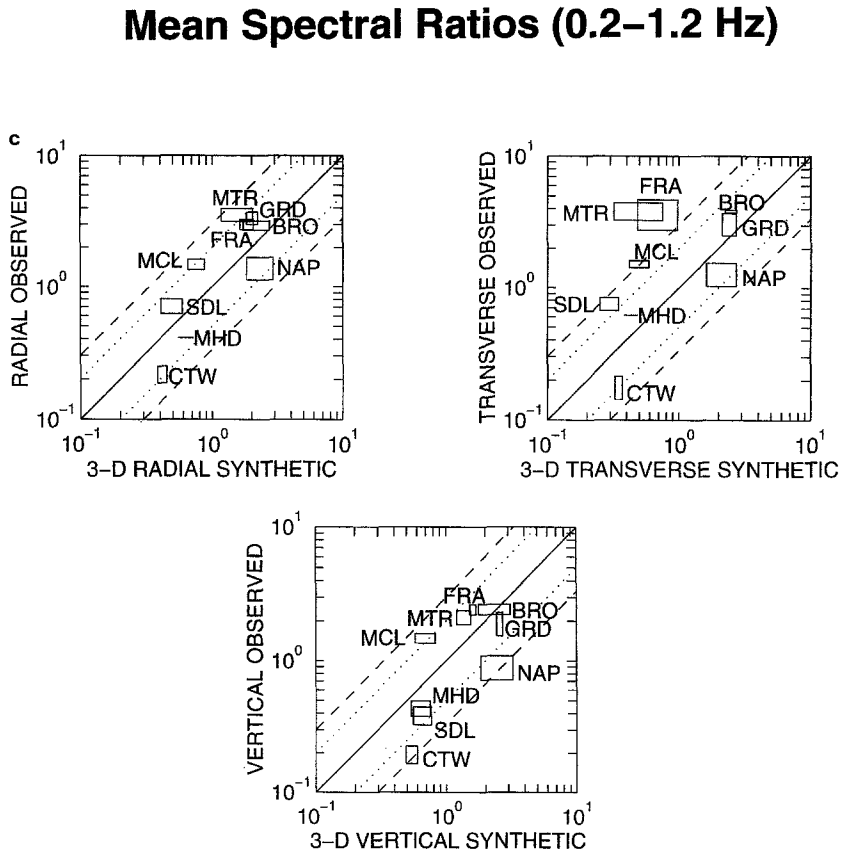

Figure 6. Graphs of observed versus 3D simulated ground-motion parameter ratios for Bingham Mine blasts: (a) peak particle velocities, (b) cumulative kinetic energies, and (c) mean spectral magnitudes. The cumulative kinetic energies for data and 3D synthetics were calculated using densities of 2.2 and 2.6 g/cm^3 for soil and bedrock sites, respectively. The values shown are for nine different stations and are normalized to the radial-component values at the rock station NOQ. See Figure 1 for station locations. The width of each rectangle is defined by the variation of the simulated parameter ratios within a 1.2 × 1.2-km square centered at the recording site. The height of each rectangle is defined by the variation of the parameters among the four recorded blasts. The dotted and dashed lines represent factor of 2 and factor of 3 discrepancies, respectively, between the observed and simulated ratios.

shows that a significant amount of energy is transferred from the radial and vertical components to the transverse component. This transverse-component energy is generated by refractions, reflections, and mode conversions at the basin walls.

We use the variations of the ground-motion parameters for the four blasts to crudely estimate the uncertainties of the ground-motion parameters. For example, the four recorded seismograms at FRAR in Figure 4 have normalized radial peak particle velocities of 5.00, 3.19, 2.24, and 4.15, so that the uncertainty range of this parameter is taken to be 2.24 to 5.00. We use a different procedure to estimate the corresponding parameter uncertainties for the synthetic seismograms. The parameter uncertainty for the synthetic seismograms at a grid point is computed from the variation of the parameter values within a 1.2 × 1.2-km horizontal square centered at that grid point. The width of this square corresponds approximately to the estimated lateral uncertainty of the basin model determined from gravity data (Radkins, 1990).

Figure 6 shows observed parameter ratios plotted against 3D synthetic parameter ratios, with their estimated uncertainties, for nine recording stations. We note that the ground-motion parameter ratios generally lie within a factor of 3 of the solid lines, which represent a perfect match between the observed and simulated ratios. The station-to-station variation in the observed ground-motion parameters is between one and two orders of magnitude, depending on the parameter. Thus, the 3D simulation reproduces the overall pattern of the spatial variations in ground motion from the blasts. However, there are some large disagreements between observed and predicted ratios of ground-motion parameters. The best agreement is obtained for the vertical-component values. In contrast, the simulated horizontal-component values tend to underestimate the observed ones, especially for the transverse component. The somewhat

larger discrepancy for the transverse component may be due to seismic energy generated by *P*- to *S*-wave conversions and reflections at rock heterogeneities and/or topographic features near the blast. Such seismic energy is absent from the wave field simulated in the two-layer basin model.

Causes of Discrepancies between Data and 3D Synthetics

This section identifies possible causes of the discrepancies between the observed and simulated records of the Bingham Mine blasts. We use 2D simulations to examine how topography and near-surface low velocities affect site amplification along a profile across the southern part of the valley. Here, we use an explosive line source located below the southwestern edge of the Bingham Mine pit, at the approximate location of three of the four recorded blasts and about 3 km west-southwest of the blast location used for the 3D simulation. We transform the synthetic line source seismograms into point source velocity seismograms by the following equation:

$$S_p(t) = \frac{1}{\sqrt{R}} \frac{d}{dt}\left[\frac{1}{\sqrt{t}} * S_l(t)\right], \qquad (4)$$

where R is the distance from the source to the receiver, * denotes convolution, and the subscripts p and l denote point source and line source finite-difference seismograms, respectively (Vidale, 1987, p. 46; Vidale and Helmberger, 1987, equations 39 and 40). This correction is applied to all of the 2D synthetics shown in this article. The 2D modeling parameters are listed in Table 4.

Discrepancies at NOQ

The comparison between the simulated (3D) and observed seismograms at NOQ in Figure 4 suggests that the two-layer Salt Lake Basin model is too simple for the bandwidth of the simulation. For example, the simulated transverse-component seismograms at NOQ contains very little energy, in contrast to the transverse-component data recorded at this station. This is because our Salt Lake Basin model between the source location and NOQ consists of homogeneous bedrock and a flat free surface, resulting in relatively simple synthetic seismograms at NOQ that are dominated by a direct *P* wave and a Rayleigh wave (Fig. 7). We expect the actual seismograms to be more complicated, due in part to scattering from bedrock velocity variations and topographic features such as the Bingham Mine pit and the Oquirrh Mountains.

Scattering by Topography

We have omitted topography in our 3D Salt Lake Basin model. However, Xu (1995) showed that topographic scattering effects from the Wasatch and Oquirrh Mountains can be significant at sites located in the adjacent Salt Lake Valley. In this section, we estimate the effects of topographic scattering on the ground-motion parameters at NOQ and along a profile in the southern part of the basin by simulating 2D wave propagation in vertical cross sections of the Salt Lake Basin model.

We select the cross section of the basin model along the profile P1-P2 (shown on Fig. 1) to examine the influence of seismic scattering from the Oquirrh Mountains at NOQ. The maximum relief between the source and NOQ along profile P1-P2 is about 575 m. Figure 8 shows the radial- and vertical-component velocity seismograms along P1-P2 com-

Table 4
2D Modeling Parameters

Spatial discretization (km)	0.025
Temporal discretization (sec)	0.0021
P-wave velocity of unconsolidated sediments (km/sec)	1.65
S-wave velocity of unconsolidated sediments (km/sec)	0.41
Density of unconsolidated sediments (g/cm^3)	2.0
P-wave velocity of semi-consolidated sediments (km/sec)	2.20
S-wave velocity of semi-consolidated sediments (km/sec)	1.27
Density of semi-consolidated sediments (g/cm^3)	2.2
P-wave velocity of bedrock (km/sec)	5.00
S-wave velocity of bedrock (km/sec)	2.89
Density of bedrock (g/cm^3)	2.6
Number of horizontal grid points	2886
Number of vertical grid points	500
Horizontal extent of model (km)	72
Vertical extent of model (km)	12
Minimum source frequency (Hz)	0.2
Maximum source frequency (Hz)	1.2
Peak source frequency (Hz)	0.6

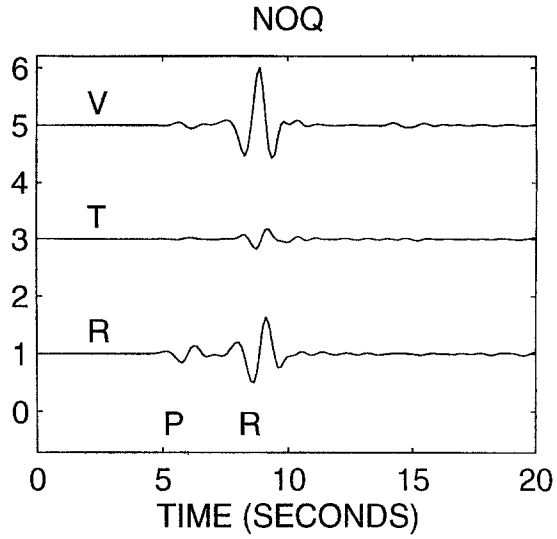

Figure 7. Vertical- (V), transverse- (T), and radial-component (R) synthetic seismograms at NOQ for a Bingham Mine blast in the simple two-layer Salt Lake Basin model. *P* denotes the direct *P* wave, and *R* denotes a Rayleigh wave.

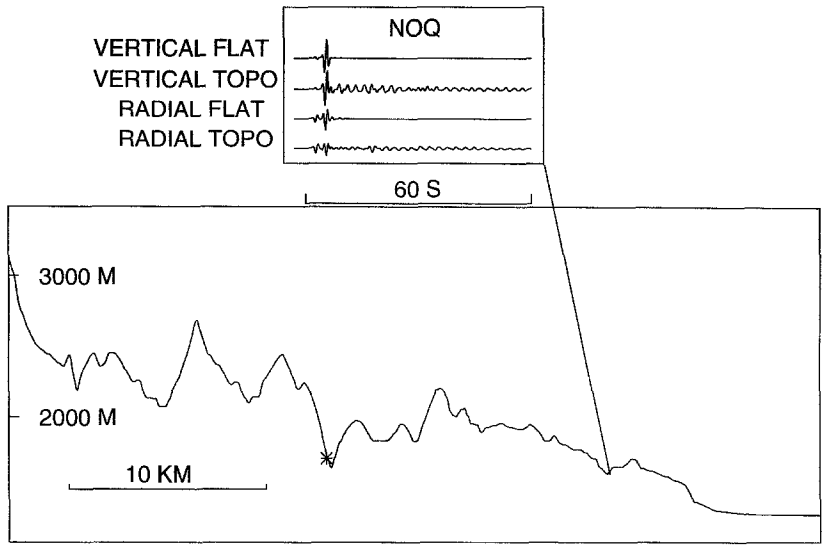

Figure 8. Radial- and vertical-component velocity seismograms at NOQ simulated using two 2D models. The two models were taken from the vertical cross section of the Salt Lake Basin model along profile P1-P2 (Fig. 1a). One model includes topography (TOPO), and the other does not (FLAT). The line source seismograms were transformed into point source seismograms by equation (4). The star depicts the location of the source, and the vertical exaggeration is 6.8.

puted, respectively, in a half-space (FLAT) and a homogeneous model with topography (TOPO). The seismograms computed in the half-space model contain only the direct *P* waves and Rayleigh waves generated by the blast. The seismograms simulated in the model with topography also contain energy scattered from the Oquirrh Mountains and show a greater similarity to the data from NOQ than do the FLAT seismograms. Relative to the half-space response, we find that topographic scattering changes the peak particle velocity, cumulative kinetic energy, and spectral magnitude at NOQ by multiplicative factors of 1.0, 2.0, and 1.3, respectively, on the vertical component, and 0.5, 1.1, and 0.9, respectively, on the radial component.

Now, we show results from 2D simulations in the vertical cross section of the Salt Lake Basin model taken along profile P3-P4 on Figure 1. Two basin models were used, one without topography and the other with topography (Fig. 9). The distances from the profile line to four alluvium sites—FRA, GRD, BRO, and MCL (≦2.1 km)—and to two rock sites—MHD and CTW (≦3.7 km)—are comparable to or less than the dominant wavelengths of *S* waves at these sites. Therefore, we can interpret the simulated ground motions at the projections of these six stations onto the profile as approximating those at the stations themselves. Figure 9 shows the radial- and vertical-component velocity seismograms simulated in the 2D basin models without mountains (*H*) and with mountains (*T*). The topographic scattering increases the normalized peak particle velocities by up to a factor of 2 relative to the response of the mountain-free model; at some sites on some components, it also increases the signal duration beyond the simulation time of 40 sec. Considering that these parameters were underestimated by the 3D synthetics for the radial and transverse components at most sites and for the vertical component at some sites (Figs. 4 and 6), we expect that the inclusion of topographic scattering in the modeling should significantly improve the accuracy of the predicted ground motions.

Effects of the Near-Surface Low-Velocity Layer

Hill and Levander (1984) and Olsen *et al.* (1995a), among others, showed that reverberations in a near-surface low-velocity layer can significantly increase the signal duration time. The near-surface unconsolidated sediments in the Salt Lake Basin were not included in our 3D model because their low seismic velocities would have increased the computer time needed for the simulation by an exorbitant amount. Borehole measurements made by Williams *et al.* (1993) 4.2 km west of BRO show average *P*- and *S*-wave velocities of 1.65 and 0.41 km/sec, respectively, in the uppermost 58 m of the sediments. These velocities are representative of the average near-surface velocities that Williams *et al.* (1993) measured in the uppermost 47 to 59 m elsewhere in the Salt Lake Basin. However, their measurements show that the average velocities over this depth range vary up to a factor of 3, at least in the northern half of the basin where 20 of their 22 boreholes were located. In our modified 2D model, *P*- and *S*-wave velocities of 1.65 and 0.41 km/sec, respectively, were assigned to the entire thickness of the unconsolidated sediments everywhere along the profile due to lack of information about the depth extent and lateral variations of these low velocities. The lower boundary of the unconsolidated sediments, R1, is a cross section along profile P3-P4 on Figure 1 of a 3D surface that we obtained by interpolating lithology information from 531 water wells in the Salt Lake Valley (Arnow *et al.*, 1970). Although the velocity contrasts at this boundary are large (Table 4), they are not unreasonable in light of the velocity-depth profiles shown in Williams *et al.* (1993).

Figure 10 shows radial- and vertical-component velocity seismograms simulated using two 2D basin models, one without the near-surface low-velocity layer and the other with it. It appears that, at some soil sites on some components, effects associated with the near-surface low-velocity layer increase the peak particle velocity by as much as a

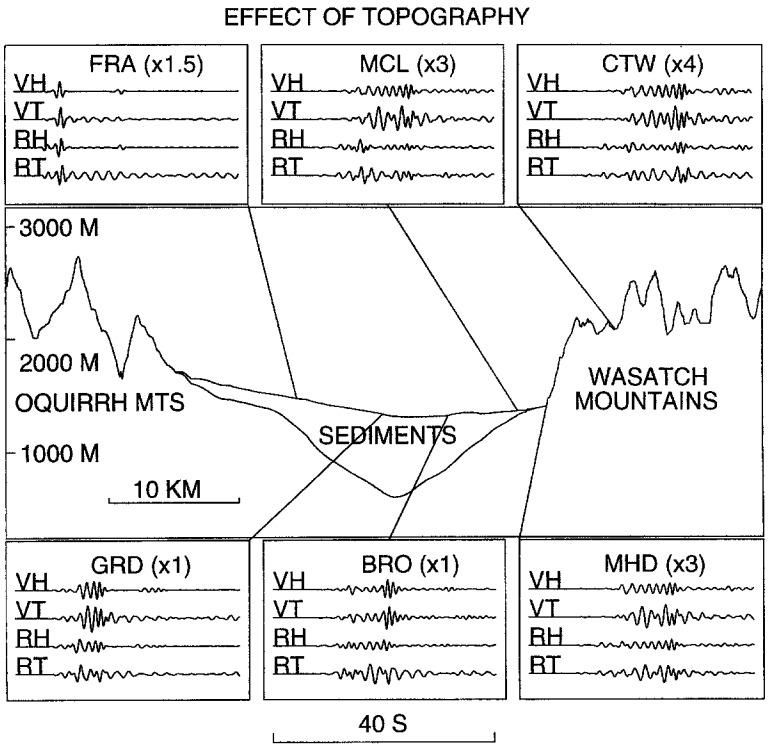

Figure 9. Radial- and vertical-component velocity seismograms simulated using 2D mountain and mountain-free basin models taken along profile P3-P4 shown on Figure 1a. The star on the cross section denotes the location of the blast. Vertical exaggeration is 8.3. *R* denotes radial component, *V* denotes vertical component, and *T* and *H* denote synthetic seismograms for the mountain and mountain-free basin models, respectively. The line source seismograms were transformed into point source seismograms by equation (4). Relative amplitude scaling factors applied for plotting clarity are indicated in parentheses.

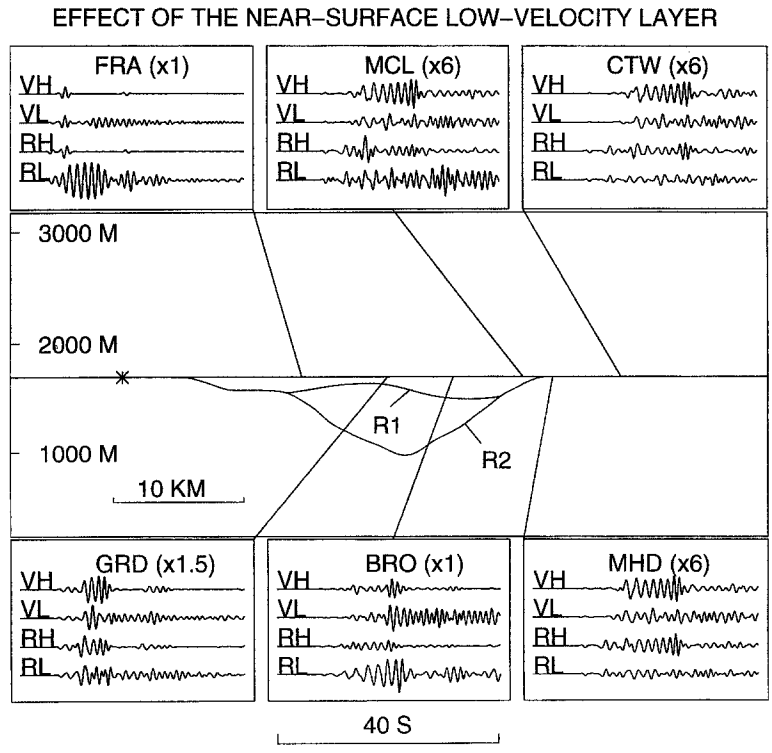

Figure 10. Radial- and vertical-component velocity seismograms simulated using two 2D basin models, one with and the other without the low-velocity layer. Both 2D models are based on the vertical cross section of the basin model along profile P3-P4 on Figure 1a. Vertical exaggeration is 8.3. The star denotes the location of the simulated blast. *R* denotes radial component, *V* denotes vertical component, and *L* and *H* denote synthetic seismograms for models with and without the near-surface low-velocity layer, respectively. The line source seismograms were transformed into point source seismograms by equation (4). Relative amplitude scaling factors applied for plotting clarity are indicated in parentheses.

factor of 3 and significantly increase the signal duration (e.g., at FRA and BRO). These increases are consistent with the findings from Olsen *et al.* (1995a), who showed that the near-surface low-velocity layer has a laterally varying resonance frequency for interference of vertically propagating *S* waves that, along this profile, generally lies within the source bandwidth of 0.2 to 1.2 Hz. Based on their findings, mode conversions and resonance are probably the main factors responsible for the larger ground motions in the simulation using the model with the near-surface low-velocity layer. Impedance effects and surface wave generation may also contribute to the amplification.

Lowpass filtering of the synthetic seismograms in Figure 10 indicates that the effects of the near-surface low-velocity layer disappear at frequencies below 0.3 to 0.4 Hz at five of the six stations. The exception is BRO, for which the effects of this layer persist down to 0.1 Hz. These observations suggest that the observed and 3D synthetic seismograms might match better at frequencies below 0.3 Hz. Unfortunately, it is not possible to test this hypothesis because all of the recorded blast signals are below the noise level in this frequency range.

Combined Effects of Topography, the Near-Surface Low-Velocity Layer, and Attenuation

The previous two sections demonstrated that topography and a near-surface low-velocity layer can each increase the amplification of peak particle velocities and signal durations in a 2D simulation by a factor of 2 or more. In this section, we present 2D synthetic seismograms computed using models that include both of these features, as well as the deep-basin structure, and that also include a correction for attenuation. We then examine how well these 2D synthetics and the ground-motion parameters computed from them fit the available blast data.

We simulated a Bingham Mine blast in 2D basin models along profiles P1-P2 and P3-P4 (Fig. 1a) that included both topography and the near-surface low-velocity layer in the sediments. We then transformed the synthetic line source seismograms into point source velocity seismograms using (4). Finally, we applied an approximate correction for attenuation using the formula

$$S(t) = S^{EL}(t) \cdot e^{-\pi f_p t/Q}, \tag{5}$$

where $S(t)$ is the corrected seismogram, $S^{EL}(t)$ is the original (elastic) seismogram, t denotes time measured from the start of the simulation, f_p represents the peak frequency of the source (0.6 Hz), and Q is the quality factor. This attenuation correction assumes that Q is the same for both P and S waves. Based on trial-and-error modeling, we chose to use Q values of 20 and 35 for seismograms simulated at soil and rock sites, respectively. For a Q of 20, the attenuation correction exceeds a factor of 2 after 8 sec.

The resulting synthetic seismograms are those labeled 2D on Figures 4a and 4c. The combined effects of topography, the near-surface low-velocity layer, and attenuation increase the signal durations at most of the soil sites and generally improve the match of the synthetic seismograms to the observed ones. Nevertheless, the waveform match between the observed and 2D synthetic seismograms is still not very good.

To what extent can the omission of topography, the near-surface low-velocity layer, and attenuation from the 3D Salt Lake Basin model account for the discrepancies between the ground-motion parameters calculated from the data and the 3D synthetics? To address this question, Figure 11 compares observed radial- and vertical-component ground-motion parameter ratios for the six stations along P3-P4 to those calculated from two sets of synthetics: the original 3D synthetics (3D seismograms in Fig. 4) and the 2D synthetics that include the effects of these three additional complexities (2D seismograms in Fig. 4). As in Figure 6, the reference values (denominators) for these ratios are the parameters computed from the radial-component records at the rock site NOQ. The uncertainty of the 2D synthetics is defined as the variation of the simulated parameter ratios within a distance of 0.5 km from the recording site. Figure 11 shows that, at most stations, the 2D synthetics computed using the more realistic basin model predict the observed ground-motion parameter ratios as well as or better than do the 3D synthetics computed with the simpler basin model. The most noticeable improvements are for the radial-component peak particle velocities and spectral magnitudes. However, the 2D radial-component cumulative kinetic energies overestimate the observed ones at BRO and FRA, whereas the corresponding 3D values do not. This mismatch is due to the much larger increase in radial component cumulative kinetic energy at FRA and BRO than at NOQ—the reference station (see radial-component seismograms in Fig. 4a). Moreover, all 2D ground-motion parameter ratios underestimate the observed ones at MCL. Except at MCL the 2D synthetics predict nearly all the observed ground-motion parameter ratios to within a factor of 3 or better—and peak particle velocity ratios to within a factor of 2 or better. The discrepancies between observed and simulated ground-motion parameter ratios are likely due to poorly constrained model parameters in the vicinity of MCL and to a lesser extent, the other stations. There are discrepancies of one sort or another at all stations.

In summary, the results from this section suggest that models used to simulate ground-motion amplification in the Salt Lake Valley should include topography, the near-surface low-velocity layer, and attenuation. Two-dimensional simulations that include these complexities are somewhat more successful at predicting ground-motion variations around the valley than 3D simulations that do not include them.

Conclusions

Our simulation of 3D elastic wave propagation in a simple two-layer model of the Salt Lake Basin is able to predict some of the overall patterns in observed amplification of ground motions from a blast at a nearby open-pit mine, as measured by peak particle velocities, cumulative kinetic energies, and spectral magnitudes normalized to values at the rock site nearest the source. However, there are order-of-magnitude discrepancies between some of the observed and predicted ratios of ground-motion parameters, and the simulations underpredict the signal durations at most stations. We use 2D simulations to explore possible causes of these discrepancies. The causes we identified may be summarized, in order of importance, as follows:

1. amplification effects associated with the low-velocity (V_p = 1.65 km/sec, V_s = 0.41 km/sec) near-surface layer of

Peak Particle Velocity Ratios

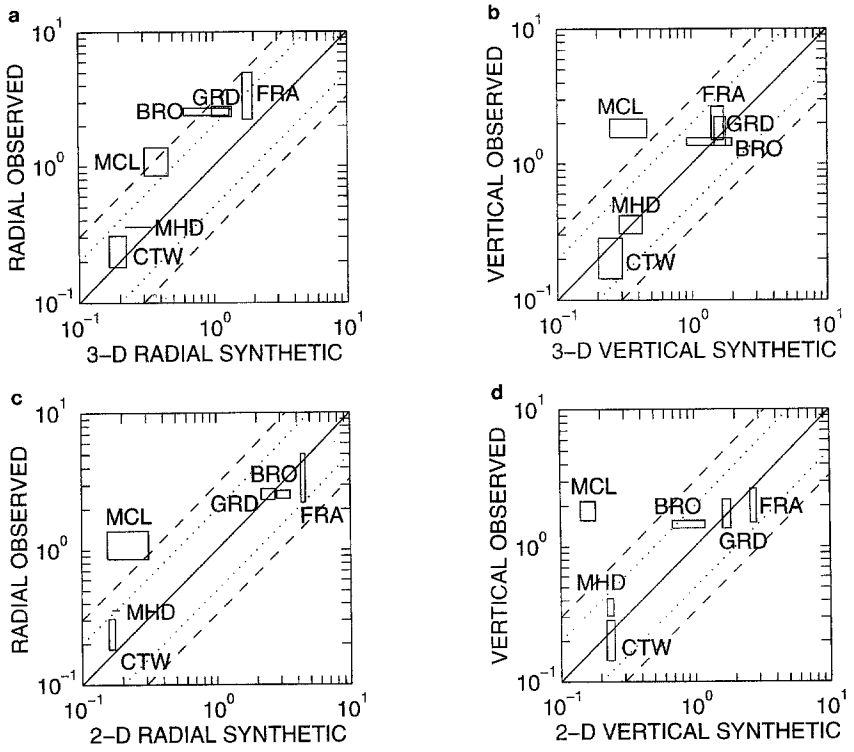

Cumulative Kinetic Energy Ratios

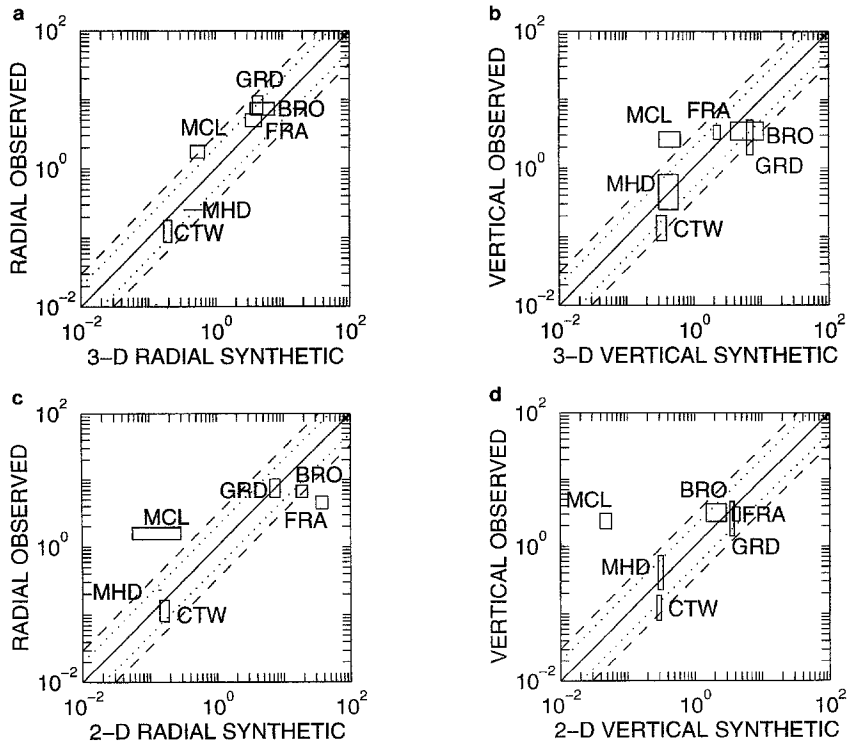

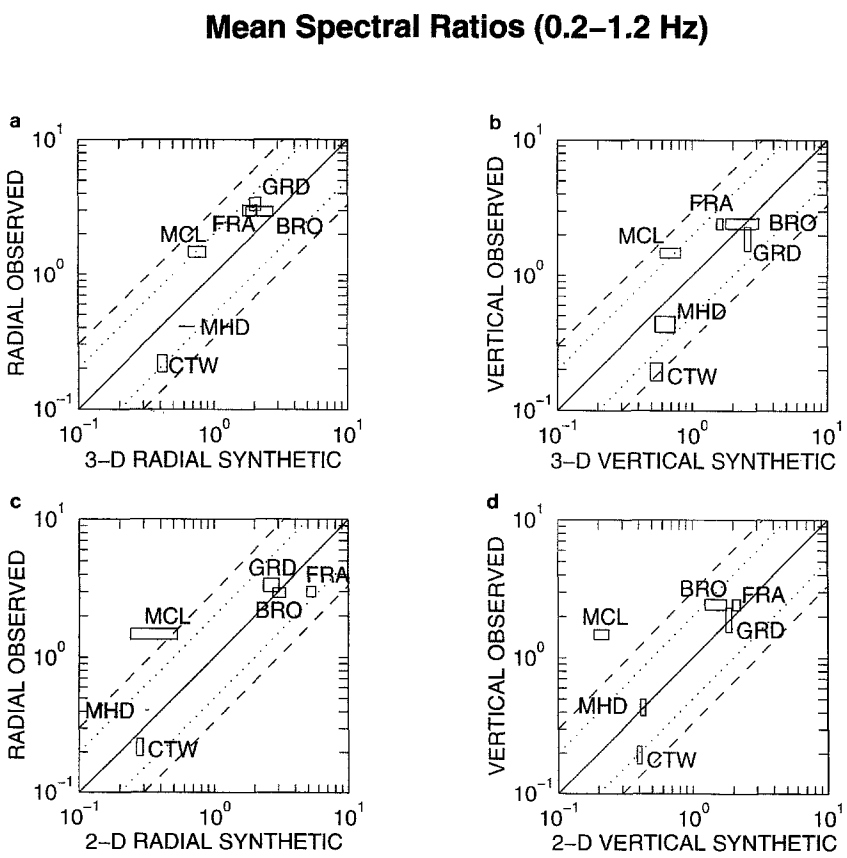

Figure 11. Graphs of observed versus simulated ratios of peak particle velocities, cumulative kinetic energies, and mean spectral amplitudes for Bingham Mine blasts. (a) Radial- and (b) vertical-component ratios for observed versus 3D synthetic seismograms. (c) Radial- and (d) vertical-component ratios for observed versus 2D synthetic seismograms. The 2D synthetics were computed using cross sections of the 3D Salt Lake Basin model along profiles P1-P2 and P3-P4 (see Fig. 1b), with topography and a near-surface sediment low-velocity layer added. The 2D synthetics were corrected for attenuation (Q equals 20 for soil sites and 35 for bedrock sites) and then transformed into point source seismograms by equation (4). For the cumulative kinetic energy calculations, we used a density of 2.6 g/cm^3 for rock sites and densities of 2.2 and 2.0 g/cm^3 for all soil sites in the 3D and 2D cases, respectively. On all plots, the values shown are for the six stations along P3-P4 only and are normalized to the radial-component values at the rock station NOQ. See Figure 1 for station locations. The width of each rectangle is defined by the variation of the simulated mean spectral ratios within a 1.2 × 1.2-km square centered at the recording site for the 3D synthetics and within a distance of 0.5 km from the recording site for the 2D synthetics. The height of each rectangle is defined by the variation of the parameters among the four recorded blasts. The dotted and dashed lines represent factor of 2 and factor of 3 discrepancies, respectively, between the observed and simulated ratios.

unconsolidated sediments, which can increase the peak particle velocities by up to a factor of 3 and increase the signal duration times significantly at soil sites along a profile in the southern part of Salt Lake Valley;

2. attenuation, which for realistic Q values (20 for soil sites and 35 for bedrock sites) greatly diminishes the signal durations on the synthetic seismograms; and
3. topographic scattering, which can double the peak particle velocities and signal durations at some sites along a profile in the sourthern part of the Salt Lake Valley.

Compared to the records from the simple two-layer 3D simulation, the records from a 2D *P/SV*-wave simulation that includes processes (1) through (3) provide a better match to the blast data recorded on the vertical and radial components. For these components, the 2D simulation predicts most of the observed peak particle velocity ratios to within a factor of 2, and most of the other observed ground-motion parameter ratios to within a factor of 3.

Our results suggest that the effects of the deep basin structure, the near-surface low-velocity layer, attenuation,

and topography on seismic wave propagation all significantly influence site amplification in the Salt Lake Basin. Future modeling of site amplification in the Salt Lake Basin should include all of these phenomena.

Acknowledgments

We gratefully acknowledge the contributions of the many people who helped us with this study. Jinlong Xu provided the 2D finite-difference code capable of handling topography at the free surface. E. McPherson and G. Henschel were responsible for calibrating, installing, and operating the seismographic instrumentation used to collect the data. K. Whipp, J. Wolfe, T. Atkin, H. Van Hooser, C. Zhou, G. P. Fivas, D. Trentman, and R. Marchant assisted with the field work. G. P. Fivas assembled the data set from the raw data tapes. D. Trentman, H. Parker, and B. Bone provided help with computer-related problems. The following landowners kindly allowed us to operate portable digital seismographs on their property: Mr. and Mrs. W. Bromley, J. Frankovich, E. F. Gardner, Mr. and Mrs. J. R. Gordon, the Great Salt Lake Council of the Boy Scouts of America, Mr. and Mrs. W. Johnson, J. Hunter, Kennecott Corporation, Mr. and Mrs. R. McClure, and R. T. Montrone. The PASSCAL program of the Incorporated Research Institutions for Seismology supplied some of the instrumentation used in this study. The University of Utah Supercomputing Institute provided computer time on an IBM 3090 for the 3D simulation. S. Larsen, D. M. Boore, and C. Ammon thoroughly reviewed the article. This work was supported by the National Science Foundation under Grant Number EAR-9104866 and by the state of Utah.

References

Arnow, T., R. Van Horn, and R. LaPray (1970). The Pre-Quaternary surface in the Jordan Valley, Utah, *U.S. Geol. Surv. Profes. Pap. 700-D,* D257–D261.

Benz, H. and R. B. Smith (1988). Elastic-wave propagation and site amplification in the Salt Lake Valley, Utah, from simulated normal faulting earthquakes, *Bull. Seism. Soc. Am.* **78,** 1851–1874.

Cerjan, C., D. Kosloff, R. Kosloff, and M. Reshef (1985). A nonreflecting boundary condition for discrete acoustic and elastic wave equations, *Geophysics* **50,**705–708.

Frankel, A. and J. Vidale (1992). A three-dimensional simulation of seismic waves in the Santa Clara Valley, California, from a Loma Prieta aftershock, *Bull. Seism. Soc. Am.* **82,** 2045–2074.

Frankel, A. (1993). Three-dimensional simulations of ground motions in San Bernardino Valley, California, for hypothetical earthquakes on the San Andreas Fault, *Bull. Seism. Soc. Am.* **83,** 1020–1041.

Graves, R. (1993). Modeling three-dimensional site response in the Marina District Basin, San Francisco, California, *Bull. Seism. Soc. Am.* **83,** 1042–1063.

Hill, J., H. Benz, M. Murphy, and G. T. Schuster (1990). Propagation and resonance of SH waves in the Salt Lake Valley, Utah, *Bull. Seism. Soc. Am.* **80,** 23–42.

Hill, N. R., and A. L. Levander (1984). Resonances of low-velocity layers with lateral variations, *Bull. Seism. Soc. Am.* **74,** 521–537.

King, K. W., W. W. Hays, and P. J. McDermott (1983). Wasatch front urban area seismic response data report, *U.S. Geol. Surv. Open-File Rept. 83-452.*

King, K. W., R. A. Williams, and D. L. Carver (1987). Relative ground response in Salt Lake City and areas of Springville-Spanish Fork, Utah, in *Assessment of Regional Earthquake Hazards and Risk Along the Wasatch Front, Utah, U.S. Geol. Surv. Open-File Rept. 87-585,* N1–N48.

Levander, A. R. (1988). Fourth-order finite-difference P-SV seismograms, *Geophysics* **53,** 1425–1436.

Murphy, M. (1989). Finite-difference simulation of seismic P- and SV-wave amplification in the Salt Lake Valley, Utah, *Master's Thesis,* University of Utah, Salt Lake City, Utah, 114 pp.

Nicholson, C. and D. W. Simpson (1985). Changes in V_p/V_s with depth; implications for appropriate velocity models, improved earthquake locations, and material properties of the upper crust, *Bull. Seism. Soc. Am.* **75,** 1105–1123.

Olsen, K. B. (1994). Simulation of three-dimensional wave propagation in the Salt Lake Basin, *Ph.D. Thesis,* University of Utah, Salt Lake City, Utah, 157 pp.

Olsen, K. B. and R. J. Archuleta (1996). Three-dimensional simulation of earthquakes on the Los Angeles fault system, *Bull. Seism. Soc. Am.* **86,** 575–596.

Olsen, K. B. and G. T. Schuster (1995). Causes of low-frequency ground motion amplification in the Salt Lake Basin: the case of the vertically-incident P wave, *Geophys. J. Int.* **122,** 1045–1061.

Olsen, K. B., J. C. Pechmann, and G. T. Schuster (1995a). Simulation of 3D elastic wave propagation in the Salt Lake Basin, *Bull. Seism. Soc. Am.* **85,** 1688–1710.

Olsen, K. B., R. J. Archuleta, and J. R. Matarese (1995b). Three-dimensional simulation of a magnitude 7.75 earthquake on the San Andreas fault, *Science* **270,** 1628–1632.

Personius, F. and W. E. Scott (1992). Surficial geologic map of the Salt Lake City segment and parts of adjacent segments of the Wasatch fault zone, Davis Salt Lake and Utah Counties, Utah, U.S. Geol. Surv. Map I-2106, scale 1:50,000.

Radkins, H. (1990). Bedrock topography of the Salt Lake Valley, Utah, from constrained inversion of gravity data, *Master's Thesis,* University of Utah, Salt Lake City, Utah, 59 pp.

Vidale, J. E. (1987). Application of two-dimensional finite-difference wave simulation to earthquakes, earth structure, and seismic hazard, *Ph.D. Thesis,* California Institute of Technology, Pasadena, California, 150 pp.

Vidale, J. and D. V. Helmberger (1987). Path effects in strong motion seigmology, in *Seismic Strong Motion Synthetics,* B. A. Bolt (Editor), Academic Press Inc, London.

Williams, R. A., K. W. King, and J. C. Tinsley (1993). Site response estimates in Salt Lake Valley, Utah, from borehole seismic velocities, *Bull. Seism. Soc. Am.* **83,** 862–889.

Xu, J. (1995). Finite-difference method for earth models with irregular free surfaces, *Master's Thesis,* University of Utah, Salt Lake City, Utah (submitted).

Yomogida, K. and J. T. Etgen (1993). 3 D wave propagation in the Los Angeles Basin for the Whittier-Narrows earthquake, *Bull. Seism. Soc. Am.* **83,** 1325–1344.

Department of Geology and Geophysics
University of Utah
Salt Lake City, Utah 84112

Manuscript received 3 January 1995.